Journal of Soils and Sediments
https://doi.org/10.1007/s11368-021-02954-7

SEDIMENT ENVIRONMENT AND POLLUTION CONTROL 2020

Availability and diffusion kinetic process of phosphorus in the water–sediment interface assessed by the high-resolution DGT technique

Yanwen Zhou[1,2,3,4] · Haixiang Wang[2] · Yinlong Zhang[1,4] · Yiwei Cai[2] · Hongbin Yin[5] · Zhen Yang[5] · Qiang Li[6] · Hezhong Yuan[2]

Received: 29 December 2020 / Accepted: 13 April 2021

Abstract

Purpose Desorption of phosphorus (P) bound to iron-containing minerals (Fe-P) is a crucial component of the eutrophication process in lakes. However, the main process and regulation mechanism of iron (Fe) and sulfur (S) on P release is little known because of a lack of in situ high-resolution data. High-resolution measurement evidence is needed to assess the availability and diffusion kinetic process of P at the water–sediment interface.

Materials and methods Soluble reactive phosphate (SRP), ferrous ion (Fe^{2+}), and sulfide (S^{2-}) fluxes through the water–sediment interface in a freshwater lake were detected using the novel double-sided diffusive gradients in thin films (DGT) technique. Different P forms in solid sediment were also measured using the sequential extraction procedure. The diffusion fluxes across the water–sediment interface and dynamic diffusion parameters between solid sediment and solution were calculated using the DGT-induced fluxes in sediments and soils (DIFS) model.

Results and discussion There was a clear decrease of the SRP_{DGT}, $Fe^{2+}{}_{DGT}$, and $S^{2-}{}_{DGT}$ fluxes from ~5 cm sediment depth to the water–sediment interface. The significant positive correlation between SRP_{DGT} and $Fe^{2+}{}_{DGT}$ fluxes in the whole profile demonstrates that Fe-P was a vitally important source of labile P in the solution phase. The significant positive fluxes of SRP_{DGT} and $Fe^{2+}{}_{DGT}$ indicated upward diffusion from the sediment particle toward the overlying water. This process further indicated the desorption and resupply of SRP and Fe^{2+} from the solid sediment phase and the synergistic effect between these two parameters. In addition, a gentler decline of R curves fitted with the DIFS model was found as the sediment depths increased, which suggesting the continuous resupply process from solid phase to pore water, especially under anaerobic conditions.

Conclusions The novel DGT technique in combination with DIFS analysis confirmed the considerable remobilization and transport capacity of labile P fractions including loosely adsorbed $MgCl_2$-P and reductive Fe-P. These pools can diffuse from sediment particles to the interstitial and the overlying water, and can be further assimilated by organisms in shallow lacustrine ecosystem.

Keywords Diffusion kinetic process · Phosphorus · Water–sediment interface · DGT technique · Fe bound P · Resupply

Responsible editor: Peifang Wang

✉ Hezhong Yuan
yuanhezhong@nuist.edu.cn

[1] College of Biology and the Environment, Nanjing Forestry University, Nanjing 210037, China

[2] Jiangsu Key Laboratory of Atmospheric Environment Monitoring and Pollution Control and Collaborative Innovation Center of Atmospheric Environment and Equipment Technology (CICAEET), School of Environmental Science and Engineering, Nanjing University of Information Science and Technology, Nanjing 210044, China

[3] Nanjing Research Institute of Ecological and Environmental Sciences, Nanjing 210013, China

[4] Collaborative Innovation Center of Sustainable Forestry in Southern China of Jiangsu Province, Nanjing Forestry University, Nanjing 210037, China

[5] State Key Laboratory of Lake Science and Environment, Nanjing Institute of Geography and Limnology, Chinese Academy of Sciences, Nanjing 210008, China

[6] Department of Soil Science, University of Wisconsin-Madison, Madison, WI 53706, USA

Published online: 21 April 2021

1 Introduction

Phosphorus (P) concentrations are strongly related to the deterioration of water quality, eutrophication occurrence, and the excessive multiplication of cyanophyta in lacustrine ecosystems (Giudice et al. 2018; Fink et al. 2018). Following intensive human activities, a large amount of P is discharged into lakes and finally accumulates in the sediments via exogenous inputs such as terrigenous runoff, agricultural fertilizer, and aquaculture (Elsbury et al. 2009; Horppila et al. 2017). As a net sink of contaminants including P, sediment can serve as endogenous sources of P to the water for several years, even after the external load of P in lacustrine ecosystem is restored to the tolerable level (Rydin 2000; Han et al. 2018). This endogenous release can resupply labile P load to the water, which is comparable to the external source (Dittrich et al. 2013). Previous studies have shown that P can desorb and release from the sediment into the water through physical and biochemical reactions including mineral phase solubility, advection, ion exchange, molecular diffusion, and redox reactions, as well as biologically mediated changes (Kim et al. 2003; Perrone et al. 2008; Shinohara et al. 2012). These processes can unbalance the aquatic environment and result in further eutrophication of the lake. Traditional sequential chemical extractions using given extractants have shown that P binds to different solid phases such as Fe, Al, Ca-containing minerals, and organic matter (OM) in the sediments in various ways, which can affect their potential for remobilization and resupply in lacustrine ecosystems (Ruttenberg 1992; Ruban et al. 1999b; Pardo et al. 2003). Precise understanding of P burial and diagenesis characteristics in the sediments and the interaction between the overlying water and the solid sediment particles is crucial for the management and recovery of eutrophic lakes.

The environmental geochemical behavior of P near the water–sediment interface in aquatic ecosystems is universally considered to be crucial because of transformations in the speciation and/or mobility (Simpson et al. 2019). These processes were induced by the dynamic actions including remobilization or sequestration from minerals or organisms present in the surface sediment (Selig 2008; Monbet et al. 2008; Cesbron et al. 2014). The water–sediment interface is often characterized by sharp gradients of different physical and chemical parameters such as pH, dissolved oxygen (DO) contents, redox potential, dissolved reactive phosphorus (DRP), and dissolved metal ions within small distances (Stockdale et al. 2009; Yuan et al. 2020a). Diffusion of DO from the atmosphere to the surficial sediment can result in an oxidized micro-zone in the water–sediment interface, which may vary in depth depending on biological activity, temperature, and DO demand. The thin oxidized zone is underlain by a reduced layer with low redox potential, in which P bound to ferric (oxy)hydroxides (FeO(OH)) may be released by the reduction of ferric to ferrous ions (Olila and Reddy 1997). Therefore, concentration of DRP in the water–sediment continuum may be predominantly controlled by the distribution of FeO(OH) via redox-mediated processes including adsorption and desorption (Chen et al. 2018). This boundary-layer transfer is an important factor affecting external and internal exchange of P (Riber and Wetzel 1987). Two basic dynamic processes are related to the release of P near the water–sediment interface. These are the resupply of solid P in the sediment to the interstitial water through the release of P from the binding sites and the upward diffusion of labile P in interstitial water via the concentration gradients near the boundary layer (Ding et al. 2013). Accurate understanding of dynamic process between the solid sedimentary phase and aqueous phase are essential for P cycling and the management and removal of excess P in lacustrine ecosystems.

The environmental geochemical behavior of iron (Fe) and sulfur (S) in the sediments can affect both mobility of P in the water–sediment continuum and the availability of P to aquatic organisms (Baldwin and Mitchell 2012; Norgbey et al. 2020). The DO content is one of the main factors controlling P cycling (Cesbron et al. 2014). The integration of P with iron oxyhydroxides (Fe(OOH) (i.e., Fe-P) is also critical for the immobilization of labile P fraction in sediment. Conversely, the reductive dissolution of P bound to Fe-containing minerals in the sediment particles under anoxic conditions is considered to be important for the release of P to the interstitial water and the subsequent diffusion into overlying water (Rooze et al. 2016). Furthermore, both microbial iron reduction and sulfate reduction will occur under anoxic conditions, and S cycling is consequently stimulated and involved in Fe-P cycling (Hall et al. 2006; Flynn et al. 2014; Wu et al. 2019). Iron reduction could induce the dissolution of Fe oxides to labile ferrous iron (Fe^{2+}), whereas sulfate (SO_4^{2-}) reduction results in the generation of H_2S (Sun et al. 2016). Ferric Fe (Fe^{3+}) and SO_4^{2-} can be simultaneously reduced by heterotrophic bacteria as terminal electron acceptors and induce the accumulation of labile Fe^{2+}, PO_4^{3-}, and sulfide (S^{2-}) (Hansel et al. 2015). This process favors the formation of secondary Fe-containing minerals such as Fe sulfides (FeS_x) and/or vivianite during anoxic episodes and the dissociation of phosphate, which can further fuel the eutrophication in lacustrine ecosystems (Egger et al. 2015). Chen et al. (2016) and Zhao et al. (2019) proposed that a high S^{2-} concentration can stimulate P mobilization in freshwater lake using the peeper technique. However, because of the heterogeneity of sediment at a small and/or microscale, simultaneous detection of the chemical components at a high spatial resolution is crucial for the examination of the environmental geochemical behaviors of these parameters, such as bioavailability and diffusion kinetic processes.

Previous studies mostly focused on ex situ chemical extraction methods for the estimation of the P, Fe, and S lability in lacustrine sediment, which were used to measure the concentration of different fractions bound to various minerals (Gao et al. 2016). Traditional chemical extraction procedures are mainly based on the response to chemical reagents by operational definition rather than on an in situ reflection of the involved analytes (Egger et al. 2016; Sun et al. 2016). Some recent studies have also focused on the biogeochemical cycling of Fe and S concerned with the P mobility in freshwater ecosystems by manipulating microcosm to mesocosm experiments (Chen et al. 2018; Sun et al. 2019). However, high-resolution in situ visual exploration of the availability, dynamics, and the remobilization characteristics of Fe, P, and S at the water–sediment interface of lakes currently remain limited.

Diffusive gradients in thin films (DGT) is a novel and in situ technique for the assessment of the potential of solute resupply of labile analytes such as PO_4^{3-}, Fe^{2+}, and S^{2-} from solid sediment phase to aqueous phase at a high spatial resolution (Zhang and Davison 1995; Alexa et al. 2009; Wang et al. 2019). A DGT device is composed of a binding layer and a diffusion layer and can maintain the flux of the solute controlled by diffusion from the interstitial water into the binding phase through the diffusion layer (Harper et al. 2000; Ding et al. 2010). The DGT-measured fractions consist of solute from interstitial water and the further resupply by the sediment solids. In brief, the uptake process of DGT simulates the dynamic interaction between solid and solution of analytes in the sediment (Santner et al. 2010). The DGT method can enable high-resolution two-dimensional (2D) distribution images of analytes and supply visual heterogeneity in sediment microstructure on a submillimeter scale (Han et al. 2017, 2018). Here, we employed the double-sided DGT (Zr-oxide DGT and ZrO-CA DGT) method alongside traditional analysis technologies for the synchronous measurement of heterogeneous changes of soluble reactive P (SRP), Fe^{2+}, and S^{2-} in the water–sediment interface in a representative lacustrine ecosystem at a high spatial resolution. Relative to independent Zr-oxide DGT and ZrO-CA DGT devices, this integrated double-sided DGT device allows synchronous measurement without destruction of the pristine sediment samples. The aims of this study were as follows: (1) to obtain high-resolution in situ visual occurrence characteristics of SRP, Fe^{2+}, and S^{2-} in the water–sediment interface using the advanced DGT technique; (2) clarify the desorption mechanism of the labile P fractions depending on Fe^{2+} variation in sediment due to the change of redox states; and (3) elaborate the resupply processes of labile P fractions from the solid sediment particles to the overlying water of the lake, which potentially fuel eutrophication, using the DGT-induced fluxes in sediments and soils (DIFS) model.

2 Material and methods

2.1 Sample collection and processing

Three sets of parallel sediment columns overlaid with undisturbed overlying water were carefully collected from representative regions (SJH1#, SJH2#, and SJH3#) using a columnar sampling instrument (acrylic glass tubes, 8-cm inner diameter) in June 2020 from Shijiuhu Lake (31° 27′–31° 32′ N, 118° 48′–118° 58′ E), a freshwater shallow lake located in the lower Yangtze River basin, Eastern China (Fig. 1). Overlying water samples were simultaneously collected simultaneously from these sites. Excessive nutrients including P were discharged into the lake through runoff and/or the river because of the increasing anthropogenic activities such as increasing agricultural activities, wastewater discharge, and aquaculture (Wang et al. 2013). As a result, P gradually deteriorates the water quality of the lake and has fueled eutrophication of the lake, which has attracted wide attention. One set of the collected sediment cores were carefully sliced into pieces at 1-cm intervals in the field. The obtained subsamples were put into a cooler, transferred to the laboratory and kept at 4°C. After freeze-drying with a lyophilizer and grinding, the sediment particles were passed through a 100-mesh sieve, after which, physicochemical parameters analysis was performed. Other undisturbed sediment columns were moved into the laboratory and used for DGT analysis and subsequent DIFS modeling.

The DO content, water depth (WD), temperature (T), electrical conductivity (EC), redox potential (Eh), and pH values of lake water were measured simultaneously in field using a portable water quality analyzer (HACH SL1000, Japan). Total P and SRP concentrations in the water were detected using molybdenum blue colorimetry (Ruban et al. 2001). Total organic carbon (TOC) content of the water sample was measured using the combustion oxidation-nondispersive infrared absorption method. After filtration through 0.45-μ. Total organic carbon (Whatman USA), the dissolved organic carbon (DOC) content was measured using a method similar to that for TOC. Finally, the total nitrogen (TN) content was detected using colorimetric method after digestion with potassium peroxodisulfate.

Interstitial water in the sediment column was collected via centrifugation for 30 min at 4500 rpm and further filtered through a 0.45-μm GF/C filter membrane (Whatman, USA). The concentration of SRP in interstitial water was measured using molybdenum blue colorimetry (Ruban et al. 2001).

2.2 DGT deployment

Two different assemblies were used for high-resolution 2D labile SRP (using Zr-oxide DGT) and sulfide (S^{2-}) and ferrous (Fe^{2+}) flux measurement (using ZrO-CA DGT) through the

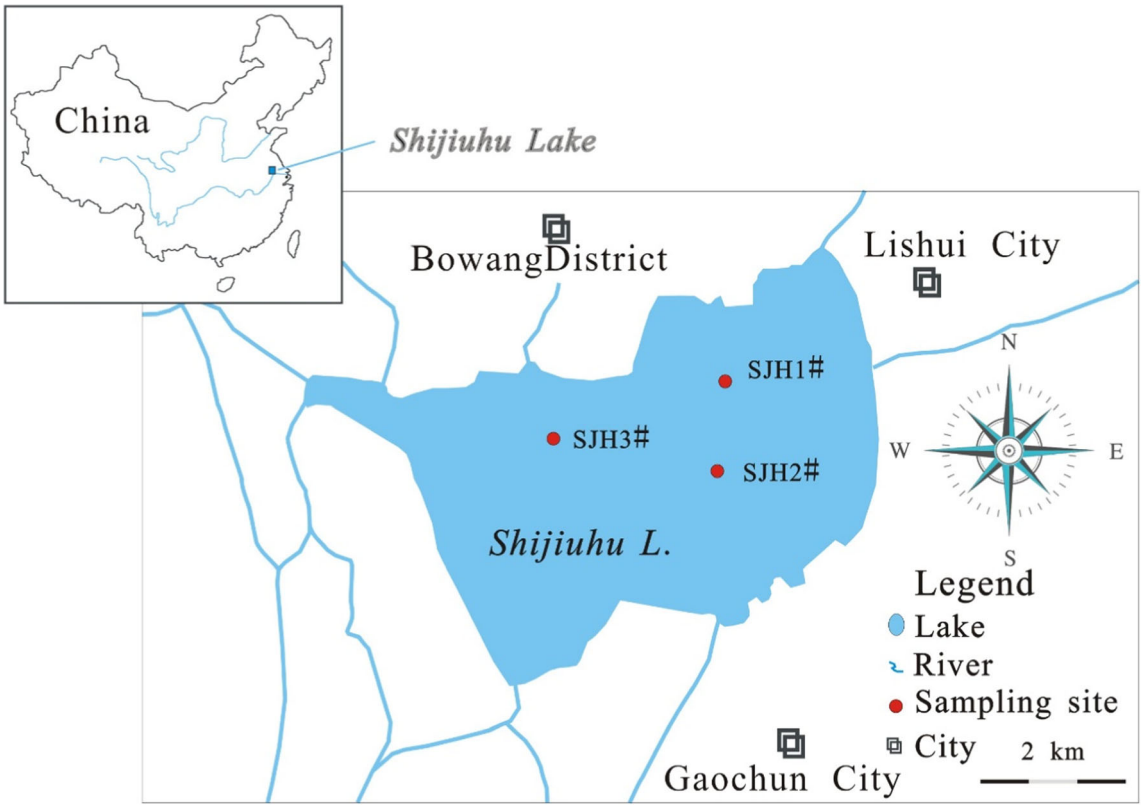

Fig. 1 Location of the research areas and the sampling sites in Shijiuhu Lake

water–sediment interface. The integrated double-sided Zr-oxide DGT and ZrO-CA DGT devices (EasySensor, China) were aerated using pure N_2 flow for 12 h for deoxidation before use. Subsequently, the DGT devices were carefully vertically inserted into sediment cores collected from Shijiuhu Lake and underwent a diffusive equilibrium period of 24 h. Subsequently, the DGT devices were removed from the sediment core, and then the gel surface was carefully rinsed using deionized (DI) water. The temperatures of the overlying water in the core were detected before and after the deployment for the calculation of diffusive flux of the analytes at the water–sediment interface.

After retrieval of the double-sided DGT assemblies from the sediment column, the DGT was separated into independent DGT devices, and the masses of P and S accumulated in the binding gels were determined separately using the modified coloration CID method (Ding et al. 2015). In brief, the gel surface of the Zr-oxide DGT and ZrO-CA DGT device was carefully rinsed using DI water and dried using filter paper. The surfaces of the gel were scanned with a flat-bed scanner (Canon 5600F, Japan) at 600-dpi resolution, which is equal to a pixel size of 42 μm × 42 μm. The obtained images were subsequently transformed into grayscale intensity with ImageJ software (free downloaded from http://rsb.info.nih.gov/ij) for the measurement of high-resolution S^{2-} fluxes. In addition, each gel from Zr-oxide DGT underlaid with wet filter paper was heated using a hot plate for 24 h at 80°C, and then soaked in the mixed molybdenum reagent for coloration (Murphy and Riley 1962) for 60 min at about 35°C. After the coloration, the DGT staining assembly was rinsed repeatedly with cool water at about 4°C and dipped in cool water for more than 5 min to stop the development of color. The surfaces of the colored hybrid film were also scanned with the flat-bed scanner (Canon 5600F, Japan) at the 600-dpi resolution for the measurement of high-resolution SRP_{DGT} fluxes. The grayscale intensities of the images after conversion to monochrome were obtained with ImageJ software. The calibration curves of the coloration CID were obtained by analyzing DGT pistons containing S^{2-} and PO_4^{3-}-P with different concentrations (Han et al. 2016). The calibration curves between accumulated masses of P and S in the gel films and grayscale intensities of corresponding analytes were fitted as exponential equations. Finally, the grayscale intensities of scanned images in sediment samples were used to calculate the S^{2-} and SRP accumulation masses for each pixel according to the observed calibration equations. The calculation method for the analyte concentration measured using DGT (C_{DGT}) was presented in Yuan et al. (2020b).

Finally, after the measurement of S^{2-} fluxes, the device surface of the ZrO-CA DGT was immediately washed using DI water, and then cut into small strips at 2-mm intervals. These subsamples were moved into the centrifuge tubes and

subsequently extracted using 1.0 mol L^{-1} nitric acid (HNO_3) at room temperature for 24 h (Chen et al. 2017; Yuan et al. 2020a). The Fe^{2+} concentration in each extract was detected using phenanthroline colorimetric methods.

2.3 Extraction of P fractions

Phosphorus pools in the sediment cores from Shijiuhu Lake were sequentially fractionated using a modified SMT (Standards Measurements and Testing Program of the European Commission) extraction scheme (Ruban et al. 1999a, 1999b, 2001). In brief, 0.2 g of dried sediment sample was soaked in different chemical extractants at a constant ratio of solid to solution (1:100) for the extraction of the P fractions. This protocol based on the operational definition of six independent procedures can differentiate the P phases in sediments into the following six major fractions: $MgCl_2$-extractable P (phase 1: $MgCl_2$-P, weakly adsorbed P; extracted using 0.1 mol L^{-1} $MgCl_2$ for 16 h); NaOH-extractable P (phase 2: Fe-P, P bound to Fe/Al oxy(hydr)oxides; extracted with 1 mol L^{-1} NaOH after phase 1 for 16 h); HCl-extractable P (phase 3: Ca-P, P associated with Ca-containing mineral; extracted with 1 mol L^{-1} HCl after phase 3 for 16 h); inorganic P (phase 4: Pi; extracted with 1 mol L^{-1} HCl for 16 h); organic P (phase 5: Po; extracted with 1 mol L^{-1} HCl for 16 h after calcination 3h at 450°C of residue from phase 4); and concentrated HCl-extractable P (phase 6: TP, extracted using 3.5 mol L^{-1} HCl for 16 h after calcining for 3h at 450°C). The phosphate concentration in the extractant was measured by molybdenum blue colorimetry.

2.4 Apparent diffusive flux calculation

The apparent diffusive flux can be used to show the diffusion direction and extent of dissolved contaminant between the overlying water and surficial sediment (Ding et al. 2015; Yuan et al. 2020a). The total diffusive flux was calculated as the sum of the fluxes from the sediments and the overlying water toward the water–sediment interface, respectively. The total fluxes were determined as follows:

$$J = J_w + J_s = -D_w\left(\frac{\partial C_{DGT}}{\partial x_w}\right)_{(x=0)} - \phi D_s\left(\frac{\partial C_{DGT}}{\partial x_s}\right)_{(x=0)} \quad (1)$$

where J is the vector sum of labile analyte (SRP, Fe^{2+}, and S^{2-}) fluxes (μg cm^{-2} s^{-1}) of the overlying water and surficial sediment. J_w and J_s represent the analyte fluxes (μg cm^{-2} s^{-1}) diffusing to the water–sediment interface from the overlying water and sediment, respectively. $(\partial C_{DGT}/\partial x_w)_{(x=0)}$ and $(\partial C_{DGT}/\partial x_s)_{(x=0)}$ represent the concentration gradients of ions in the overlying water and the sediment, respectively. The concentration gradient in this study was obtained according to the distance of 5 cm toward the water–sediment interface where x was defined as 0. φ refers to the porosity of the surface sediment. D_w and D_s represent the diffusion coefficients (cm^2 s^{-1}) in the overlying water and sediment, respectively. The D_w values can be obtained from Li and Gregory (1974), whereas D_s was obtained based on the empirical equation obtained by Ullman and Aller 1982):

$$Ds = \phi^2 D_w \quad (2)$$

2.5 DIFS model simulation

The one-dimensional (1D) DIFS model was recently employed to evaluate the diffusion kinetics of various contaminants in the sediment system and exchange between the sediment particle and the DGT interface (Harper et al. 2000; Menezes-Blackburn et al. 2016). This model can give an indication of the dependence extent of hypothetical dimensionless R (see below) on diffusion capacity of labile analytes including SRP from solid particle toward the solution (Lehto et al. 2008). This resupply process was composed of both diffusion of labile ions to the surface of DGT and further accumulation into the resin gel through the diffusion layer (Alexa et al. 2009). R can be used to reveal the resupply capacity of the analyte at the solid/solution interface and can be calculated as follows:

$$R = \frac{C_{DGT}}{C_{Pore\ water}} \quad (3)$$

where C_{DGT} is the concentration (μg L^{-1}) of labile analyte detected with DGT and $C_{Pore\ water}$ represents the SRP concentration (μg L^{-1}) in pore water gained via centrifugation.

The exchange of labile analyte between the solid sediment phase and the solution phase is governed by first-order kinetics. The governing equations consisted of a couple of linked partial differential equations (Eqs. 4 and 5) (Harper et al. 2000; Wu et al. 2016):

$$\frac{\partial C}{\partial t} = -k_1 C + K_{-1} P_c C_s + Ds\frac{\partial^2 C}{\partial x^2} \quad (4)$$

$$\frac{\partial C_s}{\partial t} = \frac{k_1 C}{P_c} - K_{-1} C_s \quad (5)$$

where K_1 and K_{-1} represent sorption constant and desorption rate constants (s^{-1}), respectively; P_c is the concentration (g cm^{-3}) of particles in sediment; and C_s refers to the concentration (mol cm^{-3}) of labile fraction of analyte in the sediment solid phase (Harper et al. 2000).

Other important kinetic parameters for DIFS model fitting for surficial sediment, used to quantify adsorption/desorption kinetics, were calculated as follows:

$$K_d = \frac{C_s}{C_{Pore\ water}} = \frac{1}{P_c} \cdot \frac{k_1}{k_{-1}} \quad (6)$$

$$T_c = \frac{1}{k_1 + k_{-1}} \quad (7)$$

where K_d represents the distribution coefficient of labile analyte fractions that can exchange with the water and T_c denotes the response time (Ernstberger et al. 2002).

The other parameters required for DIFS model fitting of surficial sediment at 5-cm depth are listed in Table 1.

2.6 Quantity control and data analyses

The glassware used in this research was washed with 5% HNO_3, and subsequent rinses using DI water. All reagents are analytical grade. The 2D and 1D spatial distribution of the SRP, S^{2-}, and Fe^{2+} fluxes across the water–sediment interface measured using DGT were generated with OriginPro 2017 64Bit (Originlab Inc., USA). Pearson correlation coefficient analysis was used for the calculation of correlation between each two variables. SPSS 20 for Windows (SPSS Inc., USA) was employed for the statistical analysis.

Table 1 Calculated input values of parameters in sediment at 5-cm depth involved in DIFS model

Site	Depth cm	Δg [a] cm	T [b] h	φ_d [c] -	φ_s [d] -	D_0 [e] $cm^2\ s^{-1}$	D_s [f] $Cm^2\ s^{-1}$	P_c [g] $g\ cm^{-3}$
SJH1#	1	0.09	24	0.75	0.845	5.74E-06	5.56E-06	0.486
	2	0.09	24	0.75	0.836	5.74E-06	5.47E-06	0.520
	3	0.09	24	0.75	0.833	5.74E-06	5.44E-06	0.533
	4	0.09	24	0.75	0.830	5.74E-06	5.41E-06	0.544
	5	0.09	24	0.75	0.830	5.74E-06	5.41E-06	0.543
	mean	**0.09**	**24**	**0.75**	**0.835**	**5.74E-06**	**5.46E-06**	**0.525**
SJH2#	1	0.09	24	0.75	0.834	5.74E-06	5.46E-06	0.526
	2	0.09	24	0.75	0.811	5.74E-06	5.24E-06	0.618
	3	0.09	24	0.75	0.819	5.74E-06	5.31E-06	0.585
	4	0.09	24	0.75	0.795	5.74E-06	5.09E-06	0.684
	5	0.09	24	0.75	0.779	5.74E-06	4.95E-06	0.754
	mean	**0.09**	**24**	**0.75**	**0.808**	**5.74E-06**	**5.20E-06**	**0.633**
SJH3#	1	0.09	24	0.75	0.856	5.74E-06	5.67E-06	0.445
	2	0.09	24	0.75	0.839	5.74E-06	5.50E-06	0.507
	3	0.09	24	0.75	0.838	5.74E-06	5.49E-06	0.514
	4	0.09	24	0.75	0.823	5.74E-06	5.34E-06	0.572
	5	0.09	24	0.75	0.818	5.74E-06	5.30E-06	0.589
	mean	**0.09**	**24**	**0.75**	**0.819**	**5.74E-06**	**5.46E-06**	**0.525**

[a] Diffusion layer thickness; [b] Deployment time; [c] Diffusion layer porosity; [d] Sediment porosity; [e] Diffusion layer diffusion coefficient; [f] Sediment diffusion coefficient; [g] Particle concentration

3 Results

3.1 Surface water properties

The key properties of overlying water from the sampling sites are presented in Table 2. Significant variation of these parameters was found between these regions. The water depth of site SJH2# was deeper than other regions. Relatively low DO concentrations were detected at site SJH2#. The highest TN, TOC, and DOC concentrations occurred at site SJH2#. High alkalinity was detected in sites SJH1# and SJH2# relative to SJH3#. A higher TP concentration was measured in site SJH2# than sites SJH1# and SJH3#. The highest SRP concentration was found at site SJH1#.

3.2 P fractions in the sediment and interstitial water

Figure 2 shows the concentration of different P pools extracted using the improved SMT method in sediment cores from different sites of the lake. In general, the recoveries of the extraction of the different P pools varied between 85 and 110%, except for a few outliers, indicating that the extraction procedure was believable. The TP, weakly adsorbed $MgCl_2$-P, Fe-P, Ca-P, Pi, and OP concentrations at three sampling sites were relatively homologous with depths, increasing in the order $MgCl_2$-P < Fe-P < Ca-P throughout the whole sediment profile. Site SJH2# had higher Fe-P values relating to its higher initial Fe concentration. Similarly, a greater Ca-P concentration was detected in majority of the sediment layers at site SJH3#, which was shown to have the higher Ca concentration. Ca-P constituted the largest fraction of 20.7 to 69.4% of the TP concentrations. A general decrease in $MgCl_2$-P, Fe-P, and Ca-P concentrations was shown with decreasing depth until water–sediment interface at sites SJH1# and SJH2#. However, there was fluctuation in the concentrations of different P phases along the entire sediment depth at site SJH3#; the concentrations for $MgCl_2$-P, Fe-P, and Ca-P upward increased until 7-cm depth and then decreased until water–sediment interface. Exchangeable $MgCl_2$-P contributed increasing fractions from 0.9 to 3.4% downward to the bottom layer. Fe-P consisted of the second largest fractions of the TP pool (22.3–41.0%). The Pi phase profile formed an approximate mirror image with Ca-P across the whole sedimentary depth and comprised larger fraction of the sedimentary P pool than Po, which was < 50%, except for few outliers. In addition, Po did not display mild vibration on the whole profile, and site SJH2# had higher Po concentrations than other lake regions. The Pi concentrations were normally higher than Po in all the sediment columns from the lake. A significantly increase of TP concentrations from 401.0 to 617.3 mg kg^{-1} toward the sediment–

Table 2 Physicochemical parameters in the overlying water of different sampling sites

Site	Location	TN mg/L	TOC	DOC	TP	SRP	DO	WD cm	EC μs/cm	Eh mV	pH
SJH1#	118° 57′ 01.08″, 31° 30′ 08.63″	0.54	1.99	0.93	0.12	0.014	6.3	60	580.0	166.0	8.6
SJH2#	118° 54′ 43.98″, 31° 28′ 53.49″	1.74	2.72	2.59	0.18	0.007	5.7	180	498.0	135.0	8.5
SJH3#	118° 53′ 27.32″, 31° 28′ 21.50″	1.08	2.82	1.65	0.17	0.008	6.5	120	501.0	198.0	6.9

water interface was found in sediment profile of site SJH3#. However, there was no clean variation of TP concentrations in sediment cores from sites SJH1# and SJH2#, with average values of 554.6±40.0 and 397.3 ±32.0 mg kg^{-1}, respectively.

3.3 High-resolution 2 D distribution of SRP and S^{2-} across the water–sediment interface

Figure 3 shows the high-resolution 2 D images of SRP and S^{2-} fluxes across the water–sediment continuum obtained using the double-sided DGT technique. Figure 4a and b shows the 1D images using this technique. In general, there were highly variable SRP and S^{2-} flux gradients throughout the water–sediment continuum at the three different sampling sites. Significantly higher fluxes were detected in the interstitial water of sediment than that in overlying water apart from S^{2-} flux in the analyzed water–sediment continuum from site SJH3#. The average SRP fluxes in overlying water were 0.009, 0.792, and 0.639 pg cm^{-2} s^{-1} at sites of SJH1#, SJH2#, and SJH3#, respectively. Higher SRP fluxes of sites SJH3# and SJH2# than site SJH1# were found except for a few outliers throughout the sediment columns. SRP fluxes of sites SJH3# and SJH2# remained relatively stable at about 35.9 ±2.6 and 37.2±1.9 pg cm^{-2} s^{-1}, respectively, from the bottom layer to about 5-cm depth layer upward, and then sharply decreased to about 2 pg cm^{-2} s^{-1} until about 2-cm depth. The fluxes then fluctuated slightly until the top layer of the sediment columns at sites SJH2# and SJH3#. A similar variation with depth was found at site SJH1#, even though there were much lower SRP fluxes in the sediment column from this site. A similar variation of S^{2-} flux to SRP flux was detected from the bottom-most to uppermost layer at sites SJH2# and SJH1#. That is, the fluxes decrease from the bottom layer to about 1-cm depth and then fluctuated upward until the top layer except for a few outliers. It is noteworthy that the S^{2-} fluxes in the surficial water in these two sites did not display major change compared with those near the water–sediment interface. Furthermore, significantly higher S^{2-} fluxes in overlying water than those in sediment were found in site SJH3#.

The SRP concentrations in pore water of sediment cores from three regions of the lake obtained using centrifugation are shown in Fig. 4e. In general, the SRP concentrations in pore water of three sampling sites were much higher than those in overlying water and decreased

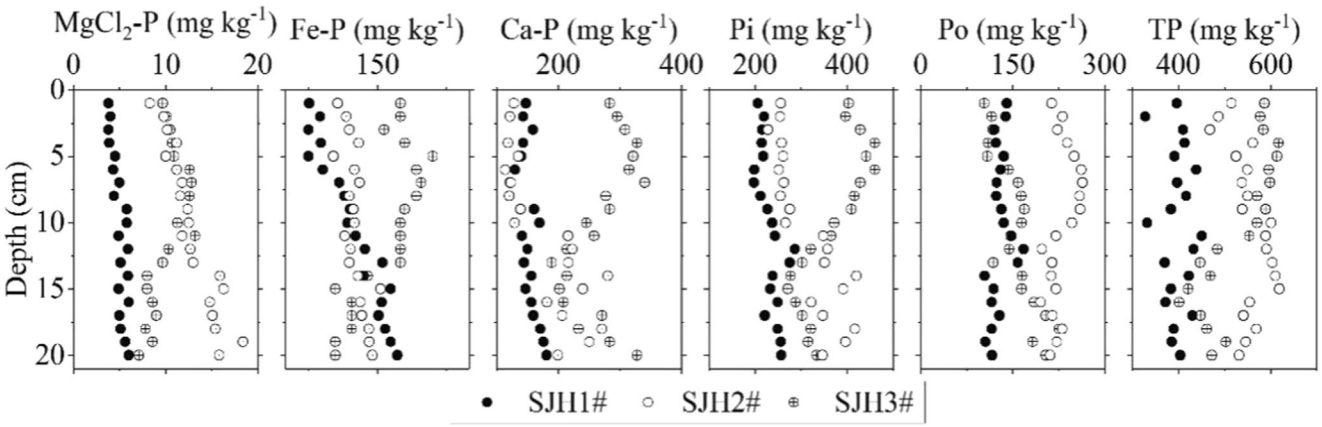

Fig. 2 Depth profiles of different P pool concentrations in the sediment of the three sampling sites

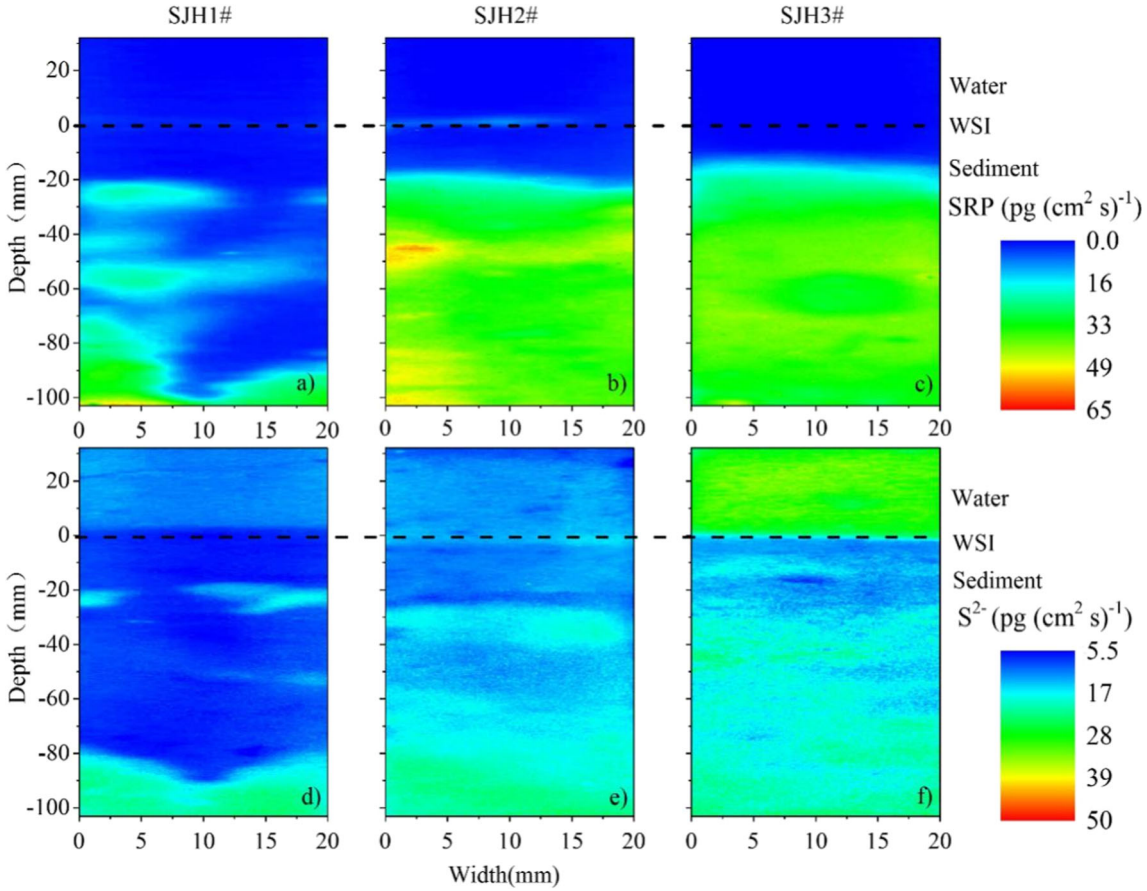

Fig. 3 High-resolution 2D images of SRP and S^2 fluxes in the water sediment continuum of the three sampling sites. The black dashed line represents the water–sediment interface (WSI)

in the following order: SJH2# > SJH1# > SJH3#. A slight decrease of the concentrations (from the bottom-most to the surface layer) from 0.73 and 0.8 mg L^{-1} to 0.42 and 0.31 mg L^{-1} was observed at sties SJH2# and SJH1#. However, such a trend was not found for site SJH3# with an average SRP concentration of 0.23 ± 0.04 mg L^{-1}.

3.4 High-resolution 1D variations of Fe^{2+} across the water–sediment interface

The 1D variation of Fe^{2+} concentrations across the water–sediment interface employing the ZrO DGT technique is shown in Fig. 4c. The Fe^{2+} concentrations at the sampling

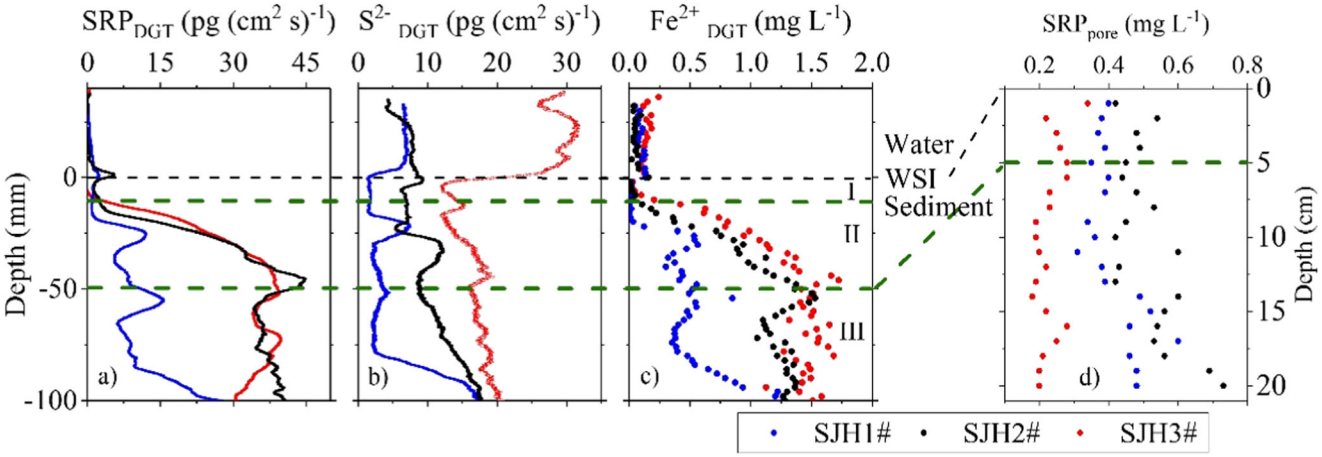

Fig. 4 High-resolution 1D profile of SRP, S^2, and Fe^{2+} fluxes obtained using DGT (**a**–**c**) and SRP concentrations in the pore water (**d**) using the centrifugation method in the water sediment continuum of the three sampling sites. The black dashed line represents the water–sediment interface (WSI). The green dashed lines represent the different variation phases on the profile of individual analytes

regions generally decrease in the order of SJH3# > SJH2# > SJH1#. Similar to SRP and S^{2-}, high variation of Fe^{2+} concentrations occurred throughout the water–sediment continuum from three different sampling sites. There was no clear variation in Fe^{2+} concentrations in sediment cores from sites SJH1# and SJH2# from the bottom-most layer to about 5-cm depth upward. A dramatic decrease of fluxes occurred from about 1.8 to about 0.01 mg L^{-1} at approximate 1-cm depth, and then remained stable until the top layer of the sediment. The Fe^{2+} concentrations of site SJH3# were distinctly lower than that of the other two regions. However, a similar variation was found at site SJH3# compared with the other two sites, in which the concentrations decreased from the bottom-most layer to about 1-cm depth from the water–sediment interface. In addition, the Fe^{2+} concentrations in overlying water were distinctly lower than those in the deep sediment and similar to those in 1-cm depth from the water–sediment interface.

3.5 Diffusion fluxes of SRP, S^{2-}, and Fe^{2+} across the water–sediment interface

Diffusion fluxes of SRP, S^{2-}, and Fe^{2+} across the water–sediment interface of the three research sites are presented in Fig. 5. There were clear positive diffusion fluxes of SRP and Fe^{2+} at all three research sites. The highest fluxes of SRP and Fe^{2+} (up to 6.9 and 0.2 μg cm^{-2} s^{-1}) were both found at sampling site SJH2#, following by site SJH3#. Significant positive S^{2-} fluxes were also measured at sites SJH2# and SJH3#. It is interesting that the S^{2-} flux was the lowest at site SJH3#, which was different from the other research sites.

4 Discussion

4.1 The importance of Fe regulation of P cycling

The variation in the proportions of the individual P fractions in the sediment indicates differences in P mobility. Relative to other P fractions, more significant positive correlations (R^2 = 0.741, 0.834, and 0.836, respectively, p<0.01) were observed between $MgCl_2$-P and Fe-P in sediment of all the sampling sites in Shijiuhu Lake (Table 3). As the most labile P form, $MgCl_2$-P represented the resupply potential of P from the sediment to the aquatic environment, including the pore water and overlying water, even the concentrations of this pool were low relative to other P fractions in the sediment. The significant positive correlation between Fe-P and $MgCl_2$-P (Table 3) indicated that Fe-P accounting for 20–67% of Pi concentration was an important source of weakly absorbed P fraction in the sediment. The higher Fe^{2+}_{DGT} and SRP_{DGT} concentrations shown in Fig. 4 were measured in the bottom-most layer of all the sediment columns, suggesting a clear resupply effect from the sediment to the solution. Van der Zee et al. (2003) proposed that the reductive dissolution of reactive FeO(OH) in the anaerobic environment in deep sediment layers can induce the release and upward diffusion of Fe^{2+} and SRP along with the re-oxidation at the water–sediment interface. This process further resulted in the diminishment of Fe^{3+} because of adsorption to solid particles on oxic/aerobic conditions, leading to sequestration of phosphate in upper sediment layer (Gächter and Müller 2003; Pagès et al. 2011). In addition, the SRP concentration in pore water measured with the centrifugation process remained relatively unchanged relative to SRP_{DGT}, indicating considerable diffusion upward via different reactions including wind disturbance in this shallow lake.

Relative to $MgCl_2$-P and Fe-P, Ca-P accounted for higher proportion of the Pi, which was more than 50% except for a few outliers, through the whole profile at the three sampling sites. High Ca-P concentrations in the sediment were also detected in Taihu Lake (Zhu et al. 2013) and Bort-Les-Orgues Reservoir (Ruban et al. 2001). However, Ca-P has been shown to be of detrital origin and to remain relatively stable during the sedimentation, without minimal release risk (Ruban et al. 1999a). Previous research based on phosphate oxygen isotopes ($\delta^{18}O_P$) in the sediment revealed that Ca-P possessed light isotope values relative to exchangeable and Fe-P, which suggests that Ca-P is locked in and remains largely unaltered after the formation and precipitation of Ca-containing minerals in the sediment (Yuan et al. 2019). Lei et al. (2020) also found consistent results during a survey to

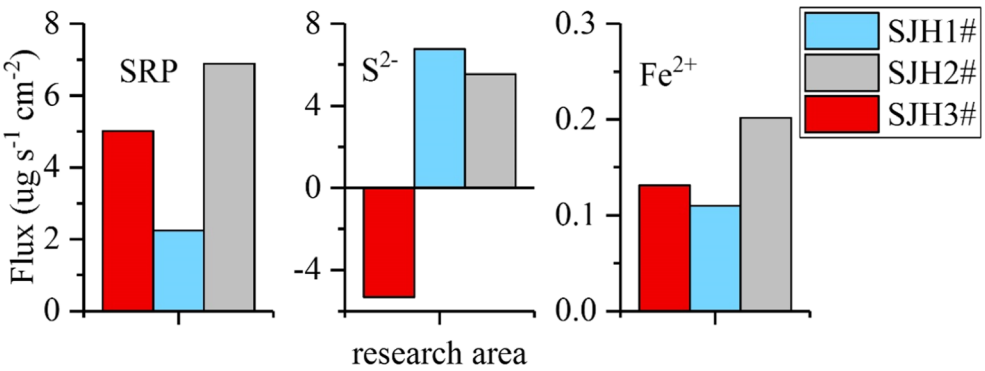

Fig. 5 Diffusion fluxes of different analytes across the water–sediment interface (WSI) at each sampling site

Table 3 Pearson correlation coefficients of individual P species in the sediments of different sites (n=20)

Site		Fraction					
SJH1#		$MgCl_2$-P	Fe-P	Ca-P	Pi	Po	TP
	$MgCl_2$-P	1.000					
	Fe-P	0.741**	1.000				
	Ca-P	0.531*	0.516 *	1.000			
	Pi	0.670**	0.705**	0.524 *	1.000		
	Po	−0.111	−0.276	−0.308	0.280	1.000	
	TP	−0.091	−0.017	−0.243	0.028	−0.338	1.000
SJH2#	$MgCl_2$-P	1.000					
	Fe-P	0.834**	1.000				
	Ca-P	0.803**	0.522 *	1.000			
	Pi	0.842**	0.593**	0.996**	1.000		
	Po	−0.376	−0.184	−0.579**	−0.565**	1.000	
	TP	0.480 *	0.342	0.624**	0.623**	−0.188	1.000
SJH3#	$MgCl_2$-P	1.000					
	Fe-P	0.836**	1.000				
	Ca-P	0.321	0.334	1.000			
	Pi	0.722**	0.767**	0.776**	1.000		
	Po	−0.415	−0.681**	−0.11	−0.432	1.000	
	TP	0.740**	0.784**	0.707**	0.949**	−0.595**	1.000

**Correlation is significant at the 0.01 level (2-tailed)

*Correlation is significant at the 0.05 level (2-tailed)

relating to $\delta^{18}O_P$ in the sediment. A weak positive correlation between Ca-P and $MgCl_2$-P (see Table 3) further indicates the inconspicuous desorption to mobile P fraction and resupply capacity for the solution. Significant positive correlations were observed between Pi and Fe-P as well as Ca-P in sediment from all sampling regions. This indicates that Fe-P and Ca-P simultaneously contributed to the Pi contents in the sediment. However, the redox-sensitive Fe-P can exert stronger influence on the cycle of Pi, even though there is a greater stock of Ca-P in the sediment.

4.2 Potential mobility of P in the water–sediment interface

Figure 5 illustrates the apparent diffusion fluxes of SRP, S^{2-}, and Fe^{2+} measured with the DGT technique across the water–sediment interface of the three sampling regions. The apparent diffusion flux can characterize the extent and direction of contaminants across the water–sediment interface (Tang et al. 2016). A positive flux represents the upward release of contaminants from the sediment system toward the overlying water of the lake, whereas a negative flux indicates that sediment is acting as a sink of contaminants from the overlying water (Ding et al. 2015). Significant positive values of the diffusion fluxes of these parameters were found except for S^{2-} at site SJH3#, indicating the diffusion direction from the surficial sediment toward the lake water in this region. Sharply downward increasing 1D SRP_{DGT} and $F^{2+}{}_{DGT}$ fluxes (Fig. 4) suggest the simultaneously desorption of phosphate and ferrous ion (Fe^{2+}) with much higher solubility than ferric ion (Fe^{3+}) from the solid sediment phase on the aggravating anaerobic conditions in the deeper layer (Heron et al. 1994). The difference in concentrations between the overlying and pore water may be responsible for the diffusive SRP_{DGT} flux at the interface by vertical molecular diffusion and convective transfer processes via a steep concentration gradient (Jensen et al. 1998; Soto-Jimenez et al. 2003). It should be noted that similar concentrations of SRP were detected in overlying water to those in the upper layer of interstitial water (Fig. 4d), suggesting that labile SRP and F^{2+} could diffuse upward into the overlying water and further induce the decreasing of SRP concentration in the interstitial water. This process dominated the positive general diffusion fluxes across the water–sediment continuum and aggravated the P load in the overlying water (Boström et al. 1988; Ignatieva 1996; Ruban et al. 1999a, 1999b).

In addition, considerable fluctuation of SRP_{DGT} and $Fe^{2+}{}_{DGT}$ fluxes was found at about 1- to 5-cm depth (phase II in Fig. 4), indicating that the desorption activity principally occurred in this layer of the sediment. This specific active layer was also observed in the water–sediment interfaces of Taihu Lake, Lake Courtille, alli di Comacchio lagoon, and

Arcachon lagoon (Azzoni et al. 2001; Hullebusch et al. 2003; Cesbron et al. 2014; Han et al. 2018). Oxygen penetration experiment revealed that the oxygen penetration depth during oxic treatment could reach about 5-cm depth and the oxygen concentration in deeper layer was lower, which can result in the reduction and desorption of Fe(III) bound P into free PO_4^{3-} and Fe^{2+} ions in the bulk sediment (Olila and Reddy 1997; Pagès et al. 2011; Yuan et al. 2020a). The strong anaerobic conditions that occurred in the layer deeper than 5 cm from the surface did not result in any major change in the labile SRP_{DGT} and $Fe^{2+}{}_{DGT}$ fluxes. This might be due to the equilibrium between continuous desorption of Fe(III) bound P in the deeper layer via reduction and resorption on reductive environment (Golterman 1995). In addition, the lack of a distinct concentration gradient was speculated to be responsible for the aggregation and accumulation of SRP_{pore} in the deep layer of the sediment. In general, an active layer of approximately 5 cm of surficial sediment in Shijiuhu Lake dominated the SRP cycle associated with the Fe-containing minerals in the lacustrine ecosystem.

Phosphorus diffusion could be driven by the release of Fe^{2+} because of the reductive dissolution of Fe(III) oxides through reaction with S^{2-} (Li et al. 2016). Sun et al. (2016) proposed that the S^{2-} accumulation with sedimentary depth could improve the P release under anoxic conditions. Fe^{2+} is generated via Fe(III) reduction by bacteria and/or S^{2-} reacting with dissolved Fe or Fe-containing minerals (Sun et al. 2016). The discrete 2D microscale zones of S^{2-} (see Fig. 3d–f) could cause the formation of FeS_x especially at deep layer of the sediment at the geological time scale (Stockdale et al. 2010). However, the limited variation of $S^{2-}{}_{DGT}$ at 5-cm depth of the sediment profile suggests that this process did not remove a substantial fraction in the studied shallow lake. Table 4 gives the Pearson correlation coefficient between SRP_{DGT}, $S^{2-}{}_{DGT}$, and $Fe^{2+}{}_{DGT}$ fluxes for the whole profile. More significant positive correlations ($R^2 > 0.94$, p=0.01) were detected between SRP_{DGT} and $Fe^{2+}{}_{DGT}$ compared with $S^{2-}{}_{DGT}$. Sulfide in interstitial water is principally generated from sulfate (SO_4^{3-}) reduction during anaerobic episodes (Naylor et al. 2004; Zhao et al. 2019). High S^{2-} production as an electron acceptor can potentially stimulate the mobility of P in the sediment (Zhao et al. 2019). However, a less S^{2-} concentration in the sediment from Shijiuhu Lake combing with the lower correlation between the $Fe^{2+}{}_{DGT}$ and $S^{2-}{}_{DGT}$ suggests that Fe^{3+} might act as preferential alternative electron acceptor for the oxidation of reactive OM into Pi in shallow lakes. This is different from the mechanisms for deep aquatic environments such as reservoirs (Norgbey et al. 2020). In general, the high-resolution DGT measurements indicate that the reduction and subsequent desorption of Fe(III)-P via abiotic and biological actions dominated the increase and the subsequent upward diffusion of SRP in the water–sediment continuum.

4.3 Resupply dynamics of SRP evaluated with the DIFS model

According to Fick's first law (Wu et al. 2018), fluxes of analytes including SRP, S^{2-}, and Fe^{2+} can be converted to the concentration in binding gel (C_{DGT}) and reflect the diffusive potential in the sediment, pore water, and DGT binding gel. The DIFS model can be employed to obtain the corresponding dynamic parameters of remobilization of phosphate in the sediment (Monbet et al. 2008). The output values of dynamic parameters including R, K_d, T_c, k_1, and k_{-1} for labile P fraction in 5-cm depths of sediment for the three study sites are shown in Table 5. The general downward increase of R with the highest values reaching up to 0.786 at research site SJH3# indicates that the depletion of $C_{pore\ water}$ can be replenished by sedimentary particles because of stronger DGT uptake in the deeper layers. Higher R values indicate a potentially higher bioavailability and resupply efficiency of labile P during the deployment time (Menezes-Blackburn et al. 2016), which are considered responsible for the higher concentrations of SRP_{pore} in deeper layer of the sediment. In addition, T_c values were subsequently calculated in the average range from 1.3×10^4 to 10.0×10^6 s at 5-cm depth except at site SJH1#, which generally decreased with the depth downward. The T_c in DIFS model can be used to characterize the sensitivity in response to the variation of R values (Monbet et al. 2008). Lower response time (T_c) in correspondence with larger R value further confirmed the potentially stronger replenishment capacity of SRP from solid particles to the interstitial water, which suggests a clear mobility and potential bioavailability of $SRP_{pore\ water}$ in the sediment system.

Table 4 Pearson correlation coefficient matrix for SRP, Fe^{2+}, and S^{2-} fluxes in sediment columns from different regions of Shijiuhu Lake (n=70)

	SJH1#			SJH2#			SJH3#		
	SRP	Fe^{2+}	S^{2-}	SRP	Fe^{2+}	S^{2-}	SRP	Fe^{2+}	S^{2-}
SRP	1	-	-	1	-	-	1	-	-
Fe^{2+}	0.967**	1	-	0.983**	1	-	0.941**[a]	1	-
S^{2-}	0.714**	0.712**	1	0.757**	0.758**	1	−0.554**	−0.500**	1

[a] Correlation is significant at the 0.01 level (2-tailed)

Table 5 Calculated output values of R, K_d, T_c, k_1, and k_{-1} for surficial sediments of different sampling sites using DIFS model

Site	Depth	R	K_d cm^3 g^{-1}	T_c s	k_1 s^{-1}	k_{-1} s^{-1}
SJH1#	1	0.020	74.66	9.999E+06	1.000E-07	2.755E-09
	2	0.020	81.79	9.999E+06	1.000E-07	2.353E-09
	3	0.158	86.84	9.999E+06	1.000E-07	2.162E-09
	4	0.055	47.24	9.999E+06	1.000E-07	3.890E-09
	5	0.091	60.94	9.999E+06	1.000E-07	3.022E-09
	mean	**0.068**	**66.56**	**9.999E+06**	**1.000E-07**	**2.720E-09**
SJH2#	1	0.026	60.03	9.999E+06	1.000E-07	3.168E-09
	2	0.064	55.91	9.999E+06	1.000E-07	2.894E-09
	3	0.279	64.73	9.999E+06	1.000E-07	2.641E-09
	4	0.404	70.35	1.601E+05	6.246E-06	1.298E-07
	5	0.561	68.35	4.935E+04	2.026E-05	3.933E-07
	mean	**0.264**	**63.74**	**9.999E+06**	**1.000E-07**	**2.456E-09**
SJH3#	1	0.005	33.77	9.999E+06	1.000E-07	6.649E-09
	2	0.324	70.76	9.929E+06	1.007E-07	2.806E-09
	3	0.605	47.31	4.092E+06	2.444E-07	1.006E-08
	4	0.786	46.69	1.298E+04	7.704E-05	2.886E-06
	5	0.383	50.01	2.219e+05	4.507E-06	1.529E-07
	mean	**0.394**	**48.06**	**1.926E+05**	**5.192E-06**	**1.976E-07**

The distribution coefficient K_d is important for the labile solid sediment phase which can exchange with the solution and, together with T_c, can also exert influence on the R values. However, no clear positive correlation was detected between K_d and T_c in this study, which could be attributed to the high influence of pH changes (Ernstberger et al. 2005). Yuan et al. (2020a) found that a low pH under anaerobic conditions in the deeper sediment layer might lead to the desorption and resupply of SRP in the sediment with higher R values. In addition, a substantially higher k_1 value than k_{-1} reflects higher potential for adsorption than desorption in the sediment (Yuan et al. 2020b). High R values together with high values of other dynamic parameters such as K_d, T_c, k_1, and k_{-1} demonstrate a continuous resupply of labile phosphate under the concentration gradient. This effect was driven by both desorption of weakly adsorbed P ($MgCl_2$-P) and the reducible fraction (i.e., Fe-P) in sediment especially under anaerobic conditions in the deep layers. This mechanism further increases the SRP concentration in overlying water and increases the P load in lacustrine ecosystems.

Finally, curves of R values over time for SRP in 5-cm sediment layers are presented in Fig. 6. The shape of the R curve of labile analytes with respect to time is mainly controlled by both the desorption capacity of sediment pellets to the interstitial water and the accompanying diffusion rate from the interstitial water toward the diffusive layer of the DGT device (Harper et al. 2000; Sochaczewski et al. 2007; Xu et al. 2012). It has been speculated that the initial rise of R curve may be due to the steeply linear diffusion gradient of mobile P fractions from the interstitial water to the diffusion layer (Monbet et al. 2008; Xu et al. 2012). After the peak of the R values, progressive decline phases occur for the majority of the sediment layers because of the limit to the resupply induced by the quick consumption of labile P near the DGT device along with the decreased desorption rate from the solid sedimentary particles (Guan et al. 2017). It is noteworthy a gentler decline of the R curves was found with the increase of depth, especially at sites SJH3# and SJH2#, which suggests a continuous resupply process from the solid phase to pore water in the deeper layer of the sediment during the deployment time until 24 h. The DIFS analysis further confirmed the considerable remobilization and transport capacity of mobile P fractions, including weakly absorbed P and reductive Fe-P, from the sediment particles to the interstitial water and overlying water via dynamic diffusion.

5 Conclusions

A novel double-sided DGT technology combing with modified SMT sequential extraction method was employed to measure the P fractions, and the fluxes of SRP_{DGT}, $Fe^{2+}{}_{DGT}$, and $S^{2-}{}_{DGT}$ in the water–sediment interface of a representative freshwater lake. It was found that Fe-P accounted for approximately 12.6–41.0% of TP represents the highest proportion of potentially mobile P. A strong increase of the high-resolution in situ SRP_{DGT}, $Fe^{2+}{}_{DGT}$, and $S^{2-}{}_{DGT}$ fluxes was shown from the water–sediment interface to approximately 5-cm depth of the sediment, indicating the high release of labile P under the anaerobic conditions. The significant positive correlation between high-resolution SRP_{DGT} and $Fe^{2+}{}_{DGT}$ fluxes through the whole profile further demonstrates that Fe-P was the main source of labile P into the solution phase in the water–sediment continuum. In addition, significant positive fluxes of SRP_{DGT} and $Fe^{2+}{}_{DGT}$ indicated upward diffusion from the sediment particles to the overlying water, showing the synergistic desorption and resupply of SRP and Fe^{2+} from the solid sediment phase. Finally, gentler decline of R curves fitted with the DIFS model was found for deeper layers, which suggests continuous resupply process from the solid phase to the pore water, especially under anaerobic conditions, and diffusion to the upper layer. Overall, the high-resolution in situ DGT technology together with DIFS kinetic analysis confirmed that a considerable remobilization effect of potentially mobile

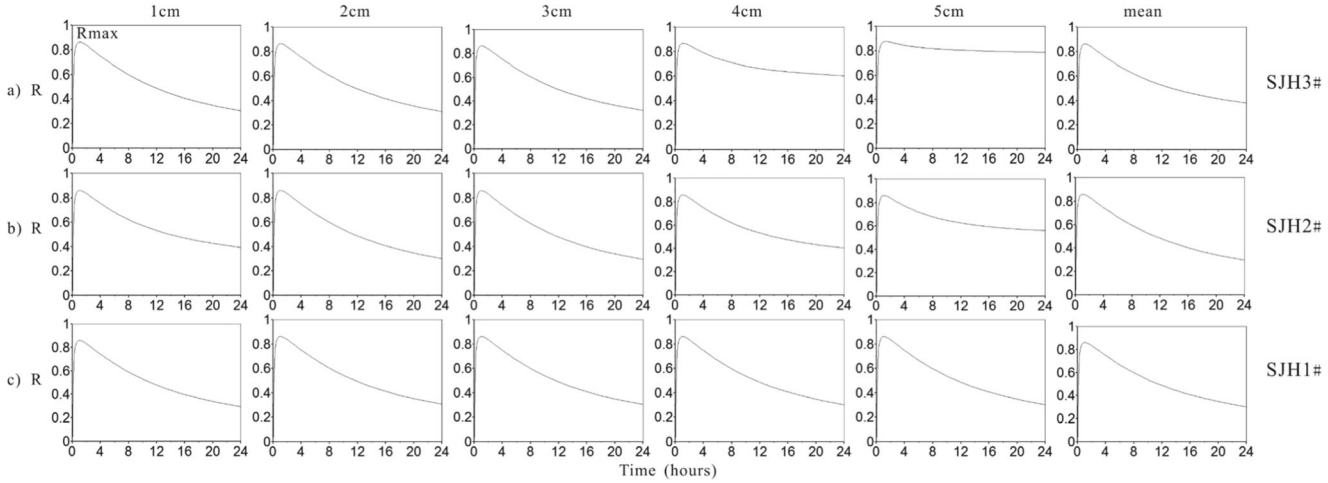

Fig. 6 Time dependence of *R* values for different sediment layers (1–5 cm) and lines fitted using the DIFS model

P fractions, including loosely adsorbed $MgCl_2$-P and reductive Fe-P from the sediment particles, dominated the resupply of labile P to the interstitial water and overlying water via dynamic diffusion. This progress is responsible for fueling the P load and potentially stimulating eutrophication in shallow lake ecosystems.

Acknowledgments We express our gratitude to Wenwen Zhang for the help of DGT analyses.

Authors' contributions Conceptualization: Yanwen Zhou, Hezhong Yuan; Methodology: Yanwen Zhou, Haixiang Wang, Hongbin Yin, Hezhong Yuan; Formal analysis and investigation: Yanwen Zhou, Haixiang Wang, Yiwei Cai, Hezhong Yuan; Writing (original draft preparation): Yanwen Zhou, Hezhong Yuan; Writing (review and editing): Qiang Li, Hezhong Yuan; Funding acquisition: Hezhong Yuan; Resources: Hongbin Yin, Zhen Yang, Hezhong Yuan; Supervision: Yinglong Zhang, Hezhong Yuan.

Funding This work was funded by National Natural Science Foundation of China (41503099; 31971476), the CAS Interdisciplinary Innovation Team (JCTD-2018-16), the Key Research Program of Frontier Sciences, CAS (ZDBS-LY-DQC018), and the Priority Academic Program Development of Jiangsu Higher Education Institutions (PAPD).

References

Alexa N, Zhang H, Lead JR (2009) Development of a miniaturized diffusive gradients in thin films (DGT) device. Anal Chim Acta 655: 80–85

Azzoni R, Giordani G, Bartoli M, Welsh DT, Viaroli P (2001) Iron, sulphur and phosphorus cycling in the rhizosphere sediments of a eutrophic *Ruppia cirrhosa* meadow (Valle Smarlacca, Italy). J Sea Res 45:15–26

Baldwin DS, Mitchell A (2012) Impact of sulfate pollution on anaerobic biogeochemical cycles in a wetland sediment. Water Res 46:965–974

Boström B, Andersen JM, Fleischer S, Jansson M (1988) Exchange of phosphorus across the sediment-water interface. Hydrobiologia 170: 229–244

Cesbron F, Metzger E, Launeau P, Deflandre B, Delgard ML, de Chanvalon AT, Geslin E, Anschutz P, Jézéquel D (2014) Simultaneous 2D imaging of dissolved iron and reactive phosphorus in sediment porewaters by thin-film and hyperspectral methods. Environ Sci Technol 48:2816–2282

Chen M, Li XH, He YH, Song N, Cai HY, Wang CH, Li YT, Chu HY, Krumholz LR, Jiang HL (2016) Increasing sulfate concentrations result in higher sulfide production and phosphorous mobilization in a shallow eutrophic freshwater lake. Water Res 96:94–104

Chen MS, Ding SM, Zhang LP, Li YY, Sun Q, Zhang CS (2017) An investigation of the effects of elevated phosphorus in water on the release of heavy metals in sediments at a high resolution. Sci Total Environ 575:330–337

Chen M, Ding S, Chen X, Sun Q, Fan X, Lin J, Ren M, Yang L, Zhang C (2018) Mechanisms driving phosphorus release during algal blooms based on hourly changes in iron and phosphorus concentrations in sediments. Water Res 133:153–164

Ding SM, Xu D, Sun Q, Yin HB, Zhang CS (2010) Measurement of dissolved reactive phosphorus using the diffusive gradients in thin films technique with a high-capacity binding phase. Environ Sci Technol 44:8169–8174

Ding SM, Wang Y, Xu D, Zhu CG, Zhang CS (2013) Gel-based coloration technique for the submillimeter-scale imaging of labile phosphorus in sediments and soils with diffusive gradients in thin films. Environ Sci Technol 47:7821–7829

Dittrich M, Chesnyuk A, Gudimov A, McCulloch J, Quazi S, Young J, Winter J, Stainsby E, Arhonditsis G (2013) Phosphorus retention in a mesotrophic lake under transient loading conditions: insights from a sediment phosphorus binding form study. Water Res 47:1433–1447

Egger M, Jilbert T, Behrends T, Rivard C, Slomp CP (2015) Vivianite is a major sink for phosphorus in methanogenic coastal surface sediments. Geochim Cosmochim Ac 169:217–235

Egger M, Kraal P, Jilbert T, Sulu-Gambari F, Sapart CJ, Röckmann T, Caroline P, Slomp CP (2016) Anaerobic oxidation of methane alters sediment records of sulfur, iron and phosphorus in the Black Sea. Biogeosciences 13:5333–5355

Elsbury KE, Paytan A, Ostrom NE, Kendall C, Young MB, McLaughlin K, Rollog M, Watson S (2009) Using oxygen isotopes of phosphate to trace phosphorus sources and cycling in Lake Erie. Environ Sci Technol 43:3108–3114

Ernstberger H, Davison W, Zhang H, Tye A, Young S (2002) Measurement and dynamic modeling of trace metal mobilization in soils using DGT and DIFS. Environ Sci Technol 36:349–354

Ernstberger H, Zhang H, Tye A, Young S, Davison W (2005) Desorption Kinetics of Cd, Zn, and Ni Measured in Soils by DGT. Environ Sci Technol 39:1591–1597

Fink G, Alcamo J, Flörke M, Reder K (2018) Phosphorus loadings to the world's largest lakes: Sources and trends. Global Biogeochem Cy 32:617–634

Flynn TM, O'Loughlin EJ, Mishra B, Dichristina TJ, Kemner KM (2014) Sulfur-mediated electron shuttling during bacterial iron reduction. Science 344:1039–1042

Gächter R, Müller B (2003) Why the phosphorus retention of lakes does not necessarily depend on the oxygen supply to their sediment surface. Limnol Oceanogr 48:929–933

Gao YL, Liang T, Tian SH, Wang LQ, Holm P, Hansen HCB (2016) High-resolution imaging of labile phosphorus and its relationship with iron redox state in lake sediments. Environ Pollut 219:466–474

Giudice DD, Zhou YT, Sinha E, Michalak AM (2018) Environ Long-term phosphorus loading and springtime temperatures explain interannual variability of hypoxia in a large temperate lake. Environ Sci Technol 52:2046–2205

Golterman HL (1995) The role of the ironhydroxide-phosphate-sulphide system in the phosphate exchange between sediments and overlying water. Hydrobiologia 297:43–54

Guan DX, Zheng JL, Luo J, Zhang H, Davison W, Ma LQ (2017) A diffusive gradients in thin-films technique for the assessment of bisphenols desorption from soils. J Hazard Mater 331:321–328

Hall KC, Baldwin DS, Rees GN, Richardson AJ (2006) Distribution of inland wetlands with sulfidic sediments in the Murray-Darling Basin, Australia. Sci Total Environ 370:235–244

Han C, Ren JH, Wang ZD, Tang H, Xu D (2017) A novel hybrid sensor for combined imaging of dissolved oxygen and labile phosphorus flux in sediment and water. Water Res 108:179–188

Han C, Ren JH, Wang ZD, Yang SK, Ke F, Xu D, Xie XC (2018) Characterization of phosphorus availability in response to radial oxygen losses in the rhizosphere of Vallisneria spiralis. Chemosphere 208:740–748

Hansel CM, Lentini CJ, Tang Y, Johnston DT, Wankel SD, Jardine PM (2015) Dominance of sulfur-fueled iron oxide reduction in low-sulfate freshwater sediments. ISME J 9:2400–2412

Harper MP, Davison W, Tych W (2000) DIFS - a modelling and simulation tool for DGT induced trace metal remobilisation in sediments and soils. Environ Model Softw 15:55–66

Heron G, Crouzet C, Bourg ACM, Christensen TH (1994) Speciation of Fe(II) and Fe(III) in contaminated aquifer sediments using chemical extraction techniques. Environ Sci Technol 28:1698–1705

Horppila J, Holmroos H, Niemistö J, Massa I, Nygrén N, Schönach P, Tapio P, Tammeorg O (2017) Variations of internal phosphorus loading and water quality in a hypertrophic lake during 40 years of different management efforts. Ecol Eng 103:264–274

Hullebusch EV, Auvray F, Deluchat V, Chazal PM, Baudu M (2003) Phosphorus fractionation and short-term mobility in the surface sediment of a polymictic shallow lake treated with a low dose of alum (Courtille Lake, France). Water Air Soil Pollut 146:75–91

Ignatieva NV (1996) Distribution and release of sedimentary phosphorus in Lake Ladoga. Hydrobiologia 322:129–136

Jensen HS, McGlathery KJ, Marino R (1998) Howarth RW. Forms and availability of sediment phosphorus in carbonate sand of Bermuda seagrass beds Limnol Oceanogr 43:799–810

Kim LH, Choi E, Michael K (2003) Sediment characteristics, phosphorus types and phosphorus release rates between river and lake sediments Stenstrom. Chemosphere 50:53–61

Lehto NJ, Sochaczewski Ł, Davison W, Tych W, Zhang H (2008) Quantitative assessment of soil parameter (K_D and T_C) estimation using DGT measurements and the 2D DIFS model. Chemosphere 71:795–801

Lei XT, Zhang H, Chen M, Guo LD, Zhang XG, Jiang ZH, Blake RE, Chen ZG (2020) The efficiency of sequential extraction of phosphorus in soil and sediment: insights from the oxygen isotope ratio of phosphate. J Soils Sediments 20:1332–1343

Li ZR, Sheng YQ, Yang J, Burton ED (2016) Phosphorus release from coastal sediments: Impacts of the oxidation-reduction potential and sulfide. Mar Pollut Bull 113:176–181

Menezes-Blackburn D, Zhang H, Stutter M, Giles CD, Darch T, George TS, Shand C, Lumsdon D, Blackwell M, Wearing C, Cooper P, Wendler R, Brown L, Haygarth PM (2016) A holistic approach to understanding the desorption of phosphorus in soils. Environ Sci Technol 50:3371–3381

Monbet P, Mckelvie I, Worsfold AJ (2008) Combined Gel Probes for the in situ determination of dissolved reactive phosphorus in porewaters and characterization of sediment reactivity. Environ Sci Technol 42: 5112–5117

Murphy J, Riley JP (1962) A modified single solution method for the determination of phosphate in natural waters. Anal Chim Acta 27: 31–36

Naylor C, Davison W, Motelica-Heino M, Van Den Berg GA, Van Der Heijdt LM (2004) Simultaneous release of sulfide with Fe, Mn, Ni and Zn in marine harbour sediment measured using a combined metal/sulfide DGT probe. Sci Total Environ 328:275–286

Norgbey E, Li YP, Ya Z, Li RH, Nwankwegu AS, Takyi-Annan GE, Luo F, Jin W, Huang YN, Sarpon L (2020) High resolution evidence of iron-phosphorus-sulfur mobility at hypoxic sediment water interface: An insight to phosphorus remobilization using DGT-induced fluxes in sediments model. Sci Total Environ 724:138204

Olila OG, Reddy KR (1997) Influence of redox potential on phosphate-uptake by sediments in two sub-tropical eutrophic lakes? Hydrobiologia 345:45–57

Pagès A, Teasdale RT, Robertson D, Bennett WW, Schäfer J, Welsh DT (2011) Representative measurement of two-dimensional reactive phosphate distributions and co-distributed iron(II) and sulfide in seagrass sediment porewaters. Chemosphere 85:1256–1261

Pardo P, Rauret G, López-Sánchez JF (2003) Analytical approaches to the determination of phosphorus partitioning patterns in sediments. J Environ Monit 5:312–318

Perrone U, Facchinelli A, Sacchi E (2008) Phosphorus dynamics in a small eutrophic Italian lake. Water Air Soil Pollut 189:335–351

Riber HH, Wetzel RG (1987) Boundary-layer and internal diffusion effects on phosphorus fluxes in lake periphyton. Limnol Oceanogr 32: 1181–1194

Rooze J, Egger M, Tsandev I, Slomp CP (2016) Iron-dependent anaerobic oxidation of methane in coastal surface sediments: Potential controls and impact. Limnol Oceanogr 61:S267–S282

Ruban D, Brigault S, Demare D, Philippe AM (1999a) An investigation of the origin and mobility of phosphorus in freshwater sediments from Bort-Les-Orgues Reservoir, France. J Environ Monit 1:403–407

Ruban V, López-Sánchez JF, Pardo P, Rauret G, Muntauc H, Quevauviller P (1999b) Selection and evaluation of sequential extraction procedures for the determination of phosphorus forms in lake sediment. J Environ Monit 1:51–56

Ruban V, López-Sánchez JF, Pardo P, Rauret G, Muntau H, Quevauviller P (2001) Harmonized protocol and certified reference material for the determination of extractable contents of phosphorus in freshwater sediments-A synthesis of recent works Fresenius. J Anal Chem 370:224–228

Ruttenberg KC (1992) Development of a sequential extraction method for different forms of phosphorus in marine sediments. Limnol Oceanogr 37:1460–1482

Rydin E (2000) Potentially mobile phosphorus in Lake Erken sediment. Water Res 34:2037–2042

Santner J, Prohaska T, Luo J, Zhang H (2010) Ferrihydrite containing gel for chemical imaging of labile phosphate species in sediments and soils using diffusive gradients in thin films. Anal Chem 82:7668–7674

Selig U (2008) Particle size-related phosphate binding and P-release at the sediment–water interface in a shallow German lake. Hydrobiologia 492:107–118

Shinohara R, Imai A, Kawasaki N, Komatsu K, Kohzu A, Miura S, Sano T, Satou T, Tomioka N (2012) Biogenic phosphorus compounds in sediment and suspended particles in a shallow eutrophic lake: A ^{31}P-nuclear magnetic resonance (^{31}P NMR) study. Environ Sci Technol 46:10572–10578

Simpson ZP, McDowell RW, Condron LM (2019) The error in stream sediment phosphorus fractionation and sorption properties effected by drying pretreatments. J Soils Sediments 19:1587–1597

Sochaczewski Ł, Tych W, Davison B, Zhang H (2007) 2D DGT induced fluxes in sediments and soils (2D DIFS). Environ Model Softw 22: 14–23

Soto-Jimenez MF, Aez-Osuna F, Bojorquez-Leyva H (2003) Nutrient cycling at the sediment–water interface and in sediments at Chiricahueto marsh: a subtropical ecosystem associated with agricultural land uses. Water Res 37:719–728

Stockdale A, Davison W, Zhang H (2009) Micro-scale biogeochemical heterogeneity in sediments: a review of available technology and observed evidence. Earth-Sci Rev 92:81–97

Stockdale A, Davison W, Zhang H (2010) Formation of iron sulfide at faecal pellets and other microniches within suboxic surface sediment. Geochim Cosmochim Acta 74:2665–2676

Sun QY, Sheng YQ, Yang J, Bonito MD, Mortimer RJG (2016) Dynamic characteristics of sulfur, iron and phosphorus in coastal polluted sediments, north China. Environ Pollut 219:588–595

Tang WZ, Duan SH, Shan BQ, Zhang H, Zhang WQ, Zhao Y, Zhang C (2016) Concentrations, diffusive fluxes and toxicity of heavy metals in pore water of the Fuyang River, Haihe Basin. Ecotoxicol Environ Saf 127:80–86

Ullman WJ, Aller RC (1982) Diffusion coefficients in nearshore marine sediments. Limnol Oceanorg 27:552–556

van der Zee C, Roberts DR, Rancourt DG, Slomp CP (2003) Nanogoethite is the dominant reactive oxyhydroxide phase in lake and marine sediments. Geology 31:993–996

Wang YH, Yang H, Chen X, Zhang JX, Ou J, Xie B, Huang CC (2013) Molecular biomarkers for sources of organic matter in lacustrine sediments in a subtropical lake in China. Environ Pollut 176:284–291

Wang Y, Yuan JH, Chen H, Zhao X, Wang DJ, Wang SQ, Ding SM (2019) Small-scale interaction of iron and phosphorus in flooded soils with rice growth. Sci Total Environ 669:911–919

Wu ZH, Wang SR, Zhang L, Jiao LX (2016) DGT induced fluxes in sediments model for the simulation of phosphorus process and the assessment of phosphorus release risk. Environ Sci Pollut Res 23: 14608–14620

Wu ZH, Wang SR, Luo J (2018) Transfer kinetics of phosphorus (P) in macrophyte rhizosphere and phytoremoval performance for lake sediments using DGT technique. J Hazard Mater 350:189–200

Wu SJ, Zhao YP, Chen YY, Dong XM, Wang MY, Wang GX (2019) Sulfur cycling in freshwater sediments: A cryptic driving force of iron deposition and phosphorus mobilization. Sci Total Environ 657:1294–1303

Xu D, Wu W, Ding SM, Sun Q, Zhang CS (2012) A high-resolution dialysis technique for rapid determination of dissolved reactive phosphate and ferrous iron in pore water of sediments. Sci Total Environ 421-422:245–252

Yuan HZ, Li Q, Kukkadapu RK, Liu EF, Yu JH, Fang H, Li H, Jaisi DB (2019) Identifying sources and cycling of phosphorus in the sediment of a shallow freshwater lake in China using phosphate oxygen isotopes. Sci Total Environ 676:823–833

Yuan HZ, Tai ZQ, Li Q, Liu EF (2020a) In-situ, high-resolution evidence from water-sediment interface for significant role of iron bound phosphorus in eutrophic lake. Sci Total Environ 706:136040

Yuan HZ, Ying HB, Yang Z, Yu JH, Liu EF, Li Q, Tai ZQ, Cai YW (2020b) Diffusion kinetic process of heavy metals in lacustrine sediment assessed under different redox conditions by DGT and DIFS model. Sci Total Environ 741:140418

Zhang H, Davison W (1995) Performance characteristics of diffusion gradients in thin films for the in situ measurement of trace metals in aqueous solution. Anal Chem 67:3391–3400

Zhao YP, Zhang ZQ, Wang GX, Li XJ, Ma J, Chen S, Deng H, Annalisa OH (2019) High sulfide production induced by algae decomposition and its potential stimulation to phosphorus mobility in sediment. Sci Total Environ 650:163–172

Zhu YR, Wu FC, He ZQ, Guo JY, Qu XX, Xie FZ, Giesy JP, Liao HQ, Guo F (2013) Characterization of organic phosphorus in lake sediments by sequential fractionation and enzymatic hydrolysis. Environ Sci Technol 47:7679–7687